Growth behavior and magnetic properties of Si_nFe ($n=2-14$) clusters

Li Ma,[1] Jijun Zhao,[2,3,*] Jianguang Wang,[1] Baolin Wang,[1,4] Qiliang Lu,[1] and Guanghou Wang[1]
[1]*National Laboratory of Solid State Microstructures and Department of Physics, Nanjing University, Nanjing 210093, China*
[2]*State Key Laboratory of Materials Modification by Laser, Electron, and Ion Beams and College of Advanced Science and Technology, Dalian University of Technology, Dalian 116024, China*
[3]*Institute for Shock Physics, Washington State University, Washington 99164, USA*
[4]*Department of Physics, Huaiyin Institute of Technology, Jiangsu 223001, China*
(Received 27 September 2005; revised manuscript received 12 December 2005; published 29 March 2006)

The growth behavior and magnetic properties of Si_nFe ($n=2-14$) clusters have been investigated using the density functional theory (DFT) within the generalized gradient approximation (GGA). Extensive search of the lowest-energy structures has been conducted by considering a number of structural isomers for each cluster size. In the ground state structures of Si_nFe clusters, the equilibrium site of Fe atom gradually moves from convex, to a surface, and to a concave site as the number of Si atoms increases from 2 to 14. Starting from $n=10$, the Fe atom completely falls into the center of the Si outer frame, forming metal-encapsulated Si cages. Maximum peaks were observed for Si_nFe clusters at $n=5$, 7, 10, 12 on the size-dependence of second-order energy difference, implying that these clusters possess relatively higher stability. The electronic structures and magnetic properties of Si_nFe clusters were discussed. We find that the magnetic moment of the Fe atom in Si_nFe clusters is quenched around the size of $n=9-10$, due to strong hybridization between the 4*s* and 3*d* states of Fe and the 3*s* and 3*p* states of Si.

DOI: 10.1103/PhysRevB.73.125439 PACS number(s): 61.46.Bc, 36.40.Cg, 73.22.−f, 71.15.Mb

I. INTRODUCTION

Silicon is the most widely used material in the microelectronic industry. The atomic structures of silicon clusters have attracted extensive theoretical and experimental attention.[1–4] Different from the carbon fullerene cages, hollow Si cage structures are unstable due to the lack of sp^2 hybridization of valence orbitals. To stabilize the silicon cages, some additional atoms stuffed inside the cage are needed to saturate the dangling bonds on the silicon cage surface and to form sp^3 hybridization. In the cases of pure Si clusters, it was found that the number of stuffed Si atoms depends on the size of the outer Si cage and the minimum cage for encapsulating Si atoms is Si_{24}.[4]

In addition to Si atoms, guest atoms of other elements like transition metals (TM) can be utilized to stabilize the hollow Si cages. Using a laser vaporization supersonic expansion technique, Beck[5] produced $TM@Si_n$ clusters and found that the doped clusters were more stable towards photofragmentation than the bare Si clusters of the same size. Hiura *et al.*[6] reported the formation of a series of Si cage clusters with endohedral transition-metal atoms, in the form of $TM@Si_n^+$, (TM=Hf, Ta, W, Re, Ir, etc.; $n=9$, 11, 12, 13, 14). Their first-principles calculations further showed that WSi_{12} is very stable due to the electronic and the geometrical shell closures.[6] It was then proposed that the metal-encapsulated Si clusters with cage configurations could act as a tunable building block for cluster-assembled materials.[6] Using mass spectrometry, a chemical-probe method and photoelectron spectroscopy, Ohara *et al.*[7] studied geometric and electronic structures of TM embedded Si clusters (TM=Ti, Hf, Mo, and W). Recently, Koyasu and co-workers[8] studied the electronic and geometrical structures of mixed-metal silicon $TMSi_{16}$ (TM=Sc, Ti, and V) clusters using mass spectrometry and anion photoelectron spectroscopy. They found that neutral $TiSi_{16}$ cluster has closed-shell electron configuration with a large gap between highest occupied molecular orbital (HOMO) and lowest unoccupied molecule orbital (LUMO).

Motivated by these experimental progresses, there have been a number of first-principles calculations of the TM-encapsulated Si cage clusters.[9–27] Kumar and Kawazoe reported computational results for metal encapsulated Si-cage-clusters.[9] They found that silicon forms fullerene-like $Si_{16}M$ (M=Hf, Zr) or cubic $Si_{14}TM$ (TM=Fe, Ru, Os) cage clusters, depending upon size of the metal atom. In their successive works, they reported a series of TM-doped Si clusters.[10–15] Khanna *et al.* investigated Cr[16] and Fe[17] encapsulating in silicon cages, and found that $Si_{12}Cr$ and $Si_{10}Fe$ are more stable than their neighbors. Both $Si_{12}Cr$ and $Si_{10}Fe$ can be explained by the 18-electron rule. Lu and Nagase[18] computed metal-doped silicon clusters $TMSi_n$ (TM=W, Zr, Os, Pt, Co, etc.) and revealed that the formation of the endohedral structure strongly depends on the size of the Si_n cluster. Based on the results from first-principles calculations, Froudakis and co-workers interpreted the structure of metal encapsulated Si cages in terms of symmetry and *d*-band filling.[19–22] Miyazaki *et al.*[23] showed that it is possible to construct a fullerene-like Si cage by doping a TM atom in the cage center. The cage is a simple 3-polytope which maximizes the number of its inner diagonals close to the metal atom. Sen and Mitas[24] reported encapsulating a TM atom in a Si_{12} hexagonal prism cage. They found the cage configuration is remarkably stable regardless of the type of doping TM atom from 3*d*, 4*d*, and 5*d* series.

In cluster physics, one of the most fundamental problems is to determine the ground-state geometry of a cluster. Although there have been many studies on the metal-doped silicon clusters in recent years,[28] there are still unclear issues in the structural and physical properties of these clusters. For

example, the initial structures of the metal-doped Si clusters were usually taken from those of the pure Si clusters and only a limited amount of structural isomers was considered for each size. Hence, some low-lying structural isomers and even the ground-state structure might be missing. Moreover, much less attention has been paid to the smaller TM-doped Si clusters (e.g., $n \leqslant 10$). It would be interesting to elucidate the growth behavior of the TM-doped Si clusters and the size-dependent evolution of physical properties of the clusters, especially the magnetic properties.

Using first-principles methods within the density functional theory (DFT), in this paper we report an extensive search for the lowest-energy configurations of $FeSi_n$ ($n=2-14$) clusters by considering a considerable amount of structural isomers. The size-dependent growth behavior and magnetic properties of the $FeSi_n$ clusters were discussed. We choose Fe atom as dopant to investigate the effect of Si cage on the magnetic moment of the transition metal impurity atom, which have significant implications in spintronic applications.[29] The rest of this paper is arranged in the following. Section II briefly describes the theoretical methods used in this work. In Sec. III, we present the lowest-energy structures and some metastable isomers of Si_nFe clusters and discuss the growth behavior of Si_nFe clusters. The electronic and magnetic properties of these clusters in ground-state structures are discussed in Sec. IV. Finally, the conclusions of this work are made in Sec. V.

II. THEORETICAL METHODS

To search the lowest-energy structures of the Si_nFe clusters, we have considered a considerable amount of possible structural isomers for each size. The number of structural candidates depends on the size of cluster. For example, thirteen initial configurations were considered for Si_7Fe, while the number of structural isomers increases to twenty for $Si_{12}Fe$. After the initial structural isomers were constructed, full geometry optimizations were performed using the spin-polarized density functional theory (DFT) implemented in a DMOL package.[30] In the electronic structure calculations, all electron treatment and double numerical basis including *d*-polarization function (DND)[30] were chosen. The exchange-correlation interaction was treated within the generalized gradient approximation (GGA) using PW91 functional.[31] Self-consistent field calculations were done with a convergence criterion of 10^{-6} Hartree Hartree on the total energy. The density mixing criterion for charge and spin were 0.02 and 0.05, respectively. The Direct Inversion in an Iterative Subspace (DIIS) approach was used to speed up SCF convergence. A 0.002 Hartree of smearing was applied to the orbital occupation. In the geometry optimization, the converge thresholds were set to 0.002 Hartree/Å for the forces, 0.005 Å for the displacement and 10^{-5} Hartree for the energy change. We started with a spin-singlet configuration for the even-electron Si_nFe clusters, spin-unrestricted calculations were then performed for all allowable spin multiplicities. The on-site charges and magnetic moment were evaluated via Mulliken population analysis.[32]

III. STRUCTURES OF CLUSTERS

Using the computation scheme described in Sec. II, we have explored a number of low-lying isomers and determined the lowest-energy structures for Si_nFe clusters up to $n=14$. The obtained ground state structures and some low-lying metastable isomers are shown in Fig. 1. The lowest-energy structures for pure Si_n clusters are also plotted in Fig. 1 for the purpose of comparison, which was reported in our recent work.[27] The geometries for pure silicon clusters agree well with previously *ab initio* calculations results,[33–36] in particular, with the results from Car-Parrinello molecular dynamics simulated annealing.[36] The binding energies (E_b), vertical ionization potentials (VIP), and HOMO-LUMO gaps for the lowest-energy structures of Si_nFe clusters are listed in Table I.

For smallest clusters with $n \leqslant 4$, both pure Si_n and Si_nFe adopt planar structures as their lowest-energy geometries. The ground-state structures of Si_2Fe and Si_3Fe can be obtained by directly adding the Fe atom to the pure Si_n clusters. An isosceles triangle (C_{2v}) was found as the ground-state structure for Si_2Fe [2(a) in Fig. 1], with two Fe–Si bonds of 2.171 Å, and one Si–Si bond of 2.256 Å, respectively. The linear chain ($C_{\infty v}$ or $D_{\infty h}$) isomers are substantially higher in energy. The ground-state structure of Si_3Fe [3(a) in Fig. 1] is a Fe-centered rhombus (C_{2v}), which is only lower than that of the three-dimensional tetrahedron (C_{3v}) [3(b) in Fig. 1] by 0.052 eV. In the case of $n=4$, the pure Si_4 adopts a rhombus with D_{2h} symmetry structure [4(a_0) in Fig. 1]. The ground-state structure of Si_4Fe is a Fe-centered trapezia (C_{2v}) [4(a) in Fig. 1]. A three-dimensional (3D) square pyramid (C_{4v}) with Fe atom on the top [4(b) in Fig. 1] was found as a metastable isomer, with only 0.035 eV higher than the ground state. Other low-lying isomers, such as Fe-centered rectangle and square, are substantially higher in energy.

As cluster size increases, 3D configurations prevail and become the ground states for both Si_n and Si_nFe clusters with $n \geqslant 5$. The structure of pure Si_5 [5(a_0) in Fig. 1] is a trigonal bipyramid (D_{3h}). A square bipyramid with Fe atom on the vertex (C_{4v}) was obtained as the lowest-energy structure for Si_5Fe [5(a) in Fig. 1]. All the other structural isomers studied are energetically unfavorable, with more than 1.5 eV energy difference from the ground state.

The lowest-energy structure obtained for Si_6 [6(a_0) in Fig. 1] is a distorted edge-capped trigonal bipyramid (C_{2v}). Two low-lying structures that are very close in energy were found for Si_6Fe, one with C_{5v} symmetry [6(a) in Fig. 1], another with C_{2v} symmetry [6(b) in Fig. 1]. Both structures are pentagonal bipyramid, while Fe atoms occupy different sites, i.e., on the vertex (C_{5v}) or on the pentagonal ring (C_{2v}). The former one is lower in energy by only 0.035 eV. Other isomers based on Fe-capped on octahedron [6(c) in Fig. 1] or trigonal prism [6(d) in Fig. 1] were obtained. Planar Fe-centered hexagon (D_{6h}) [6(e) in Fig. 1] was also found and its energy is high by 0.98 eV.

For Si_7, we obtained a pentagonal bipyramid with D_{5h} symmetry [7(a_0) in Fig. 1]. The ground-state structure obtained for Si_7Fe is a distorted cube with C_s symmetry [7(a) in Fig. 1]. For all the structural isomers shown in Fig. 1, the Fe atom locates at the vertex site.

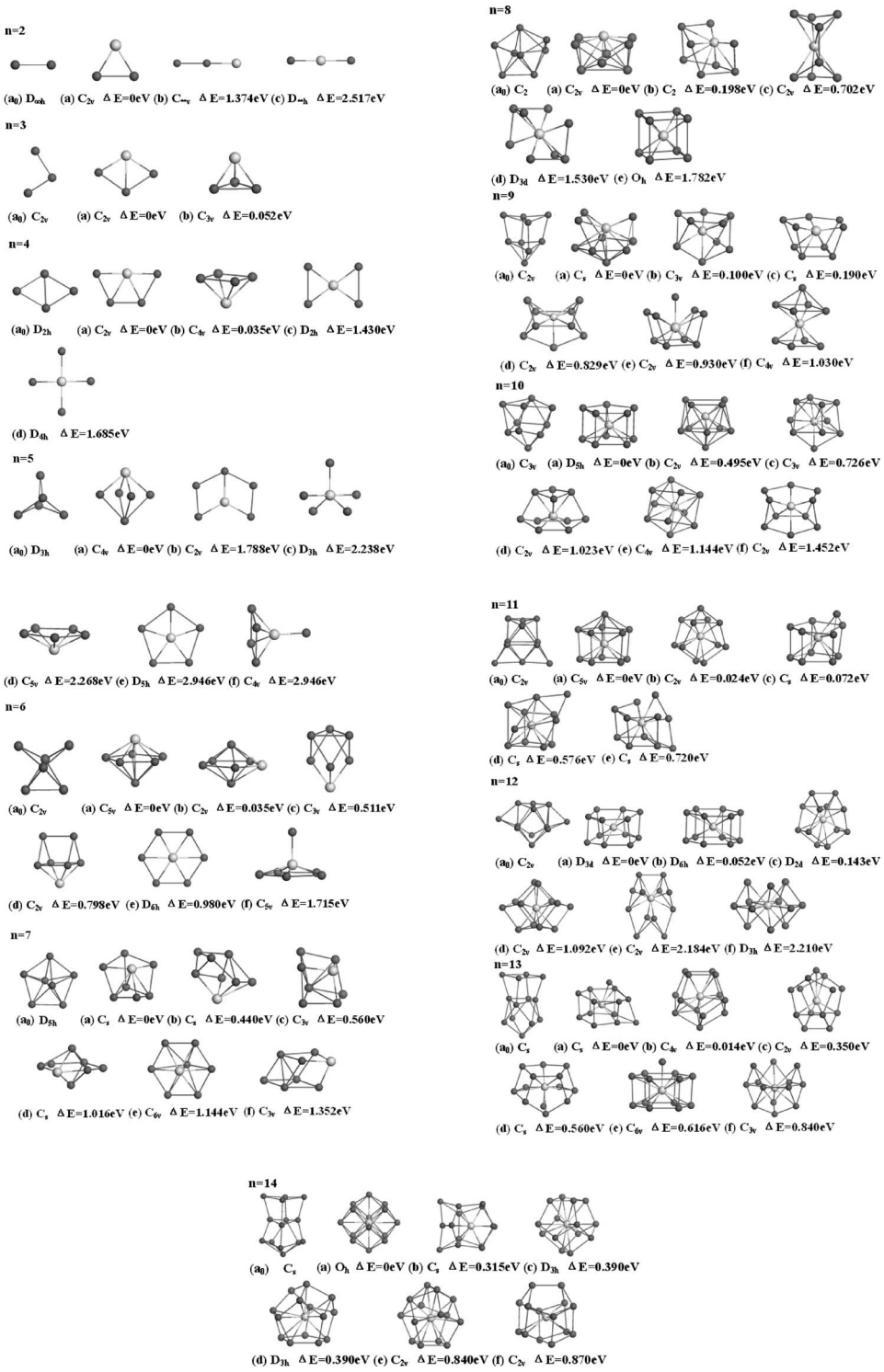

FIG. 1. The lowest-energy and low-lying structures of Si_nFe ($n=2-14$) clusters and ground-state structures of pure Si_n ($n=2-14$) clusters. Dark ball: Silicon atoms; light ball: Iron atoms. The differences of total binding energies of an isomer from the most favorable isomer are given below the structure for each size.

The lowest-energy configuration of Si_8 can be obtained by capping one Si atom on the pentagonal bipyramid of Si_7 [8(a_0) in Fig. 1]. A cage-like structure with Fe atom on the surface site (C_{2v}) was obtained as the ground-state structure for Si_8Fe [8(a) in Fig. 1]. We also considered the isomer of Fe-centered cubic structure with O_h symmetry [8(e) in Fig. 1]. But its energy is higher than the ground state by 1.782 eV. Several other isomers were considered and the Fe atom usually locates in the interior of the structure. For example, a distorted cube with Fe atom near the center [8(b) in Fig. 1] is a low-lying structure and is only 0.198 eV higher in energy.

TABLE I. Binding energy per atom (E_b), vertical ionization potential (VIP), HOMO-LUMO gap of Si_nFe clusters, atomic charges at the Fe atom, magnetic moment of the Fe atom, and total magnetic moment of Si_nFe clusters for the lowest-energy structures.

Cluster	E_b (eV)	V.I.P (eV)	Gap (eV)	Charge (e)	Magnetic moment on Fe (μ_B)	Total magnetic moment (μ_B)
Si_2Fe	2.733	7.317	0.444	−0.034	2.438	2.052
Si_3Fe	3.033	7.669	1.299	−0.067	2.492	2.006
Si_4Fe	3.070	7.235	0.636	0.087	1.911	1.909
Si_5Fe	3.465	7.871	1.468	0.048	2.421	2.013
Si_6Fe	3.433	7.593	0.712	0.129	2.093	1.797
Si_7Fe	3.570	7.124	0.626	0.179	1.987	1.957
Si_8Fe	3.597	7.402	1.211	0.206	2.140	1.990
Si_9Fe	3.692	7.397	1.000	0.526	0	0
$Si_{10}Fe$	3.773	7.248	0.900	0.585	1.140	0.880
$Si_{11}Fe$	3.769	7.161	1.208	0.632	0	0
$Si_{12}Fe$	3.851	6.671	1.156	0.482	0	0
$Si_{13}Fe$	3.822	7.092	1.080	0.616	0	0
$Si_{14}Fe$	3.866	7.095	1.481	0.612	0	0

A capped square prism is obtained for pure Si_9 [9(a_0) in Fig. 1]. For Si_9Fe cluster, all isomers have basket-like structures and Fe atom occupies the interior site. The lowest-energy structure of Si_9Fe [9(a) in Fig. 1] can be viewed as a pentagonal bipyramid face-capped by three Si atoms (C_s). A pentagonal pyramid with four capped atoms (C_{3v}) was obtained as metastable structure [9(b) in Fig. 1] and is only 0.1 eV higher in energy. Another low-lying isomer is a two-layered basket by a pentagon and a trapezia encapsulated with a Fe atom [9(c) in Fig. 1], with 0.19 eV higher in total energy.

Starting from $n \geqslant 10$, the Si_nFe clusters adopt cage-like structures with Fe atom encapsulated in the interior site. For $Si_{10}Fe$, the ground state is a Fe centered pentagonal prism with D_{5h} symmetry [10(a) in Fig. 1]. Similar to the lowest-energy structure of Si_9Fe, two low-lying isomers (C_{2v} and C_{3v}) [10(b) and 10(c) in Fig. 1] were found, both are based on a two-layered Si cage with trapezia and pentagon on each layer and one additional Si atom on the bottom. Lu[18] and Mpourmpakis[21] also obtained pentagonal prism as the ground-state structure for $Si_{10}Fe$ cluster using Becke three parameter Lee–Yang–Parr (B3LYP) functional.

The lowest-energy structure of $Si_{11}Fe$ [11(a) in Fig. 1] can be obtained by capping one Si atom on the top of Fe-centered pentagonal prism of $Si_{10}Fe$. Similarly, the metastable isomers [11(b) and 11(c) in Fig. 1] can be obtained by capping one Si atom on the face (C_{2v}) or edge (C_s) of the pentagonal prism of $Si_{10}Fe$, which are very close in energy to the ground state by only 0.024 and 0.072 eV. Khanna *et al.*[17] calculated Fe encapsulated Si_n clusters containing 9–11 Si atoms using linear combination of atomic orbitals (LCAO) molecular orbital theory with Gaussian and numerical basis functions. The lowest-energy structures obtained from their calculations are indeed low-lying isomers in our study, i.e., 9(d) and 10(c) in Fig. 1, which are higher than the present ground-state structures by 0.829 and 0.726 eV.

Similar to the pentagonal prism of $Si_{10}Fe$, Fe-centered hexagonal prism was obtained for $Si_{12}Fe$ as lowest-energy structure. However, a distorted hexagonal prism (D_{3d}) [12(a) in Fig. 1] is slightly lower than the perfect hexagonal prism (D_{6h}) [12(b) in Fig. 1] by 0.052 eV, in agreement with previous calculation by Sen and Mitas.[24] A distorted pentagonal prism with a Si dimer capped on the side (D_{2d}) [12(c) in Fig. 1] was found as low-lying isomer with $\Delta E = 0.143$ eV, which can be viewed as a continuation of the structural pattern of the metastable structure 11(b) of $Si_{11}Fe$.

For $n=13$, the lowest-energy structure of $Si_{13}Fe$ [13(a) in Fig. 1] is a distorted hexagonal prism with one Si atom on the top (C_s). The metastable structure (C_{4v}) [13(b) in Fig. 1] is also a continuation of the structural pattern of $n=11$(b) and $n=12$(c), with three Si atoms capped on the side of the distorted pentagonal prism (0.014 eV higher in energy). Another low-lying structure [13(c) in Fig. 1] is a continuation of the structural pattern of $n=12$(c) with a Si atom capped on the opposite site of Si dimer, with 0.35 eV higher in energy.

The lowest-energy structure for $Si_{14}Fe$ [14(a) in Fig. 1] is a cubic cage with Fe atom in the center (O_h). This is the same as previous result from DFT plane-wave pseudopotential calculation.[9] As shown in Fig. 1, all the structural isomers for $Si_{14}Fe$ have the cage configurations with Fe atom encapsulated in the center.

Comparing to those of pure Si_n clusters, there is substantial structural reconstruction after encapsulating Fe atom. Generally speaking, we found that the Fe atom in the lowest-energy configuration gradually moves from convex, to surface, and to the interior site as the number of Si atom varying from 2 to 14. Starting from $n=10$, the Fe atom in $Si_{10}Fe$ cluster completely falls into the center of the Si frame and form a cage. Similar behavior was observed in the $TaSi_n$ ($n=1-13$) clusters,[25] while the cage-like structure formed at $n=12$. Kawamura *et al.*[14] investigated growth behavior of metal-doped silicon clusters $TMSi_n$ (TM=Ti,Zr,Hf; $n=8-16$). They found for $n=8-12$, basketlike open structures are most favorable, while for $n=13-16$, the metal atom is completely surrounded by silicon atoms. Such difference in

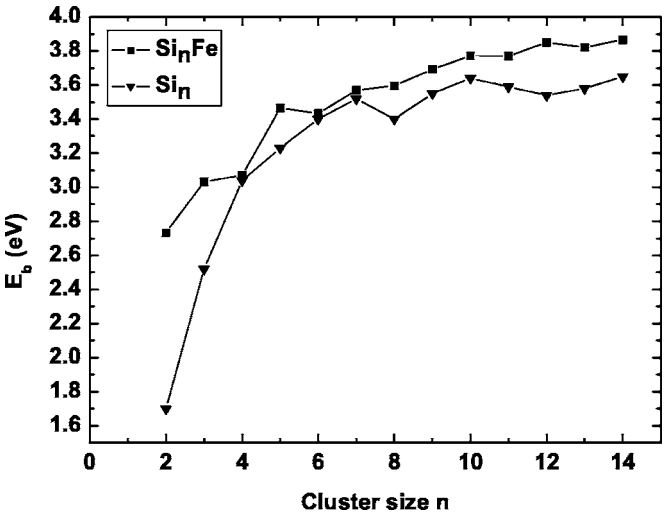

FIG. 2. Size dependence of the binding energy per atom E_b for the lowest-energy structures of Si_nFe and Si_n clusters.

the critical sizes for the formation of Si cage in various $TMSi_n$ clusters can be understood by the radius of the metal atom. Since Ta, Ti, Zr, and Hf atoms are bigger than the Fe atom, more Si atoms are needed to encapsulate the transition-metal atom completely. These findings further confirm that the metal-doped silicon clusters are favorable of forming endohedral cage-like structures and the lowest-energy configurations depend on the size of metal atom and the number of Si atoms.

IV. ELECTRONIC AND MAGNETIC PROPERTIES

We now discuss size-dependent physical properties of these clusters. The binding energies (E_b), the second-order energy differences, and the HOMO-LUMO gaps for the lowest-energy structures of Si_nFe clusters are plotted in Figs. 2–4, respectively. From Fig. 2, it can be seen that the binding energy generally increases with cluster size. Thus, the clusters can continue to gain energy during the growth process. Local peaks are found at $n=5,10,12$, implying that these clusters are more stable than their neighboring clusters. The binding energies for pure Si_n clusters[27] are also plotted in Fig. 2 for comparison. The binding energies of Si_nFe clusters are larger than those of pure Si_n. In other words, the doping of Fe atom improves the stability of silicon clusters.

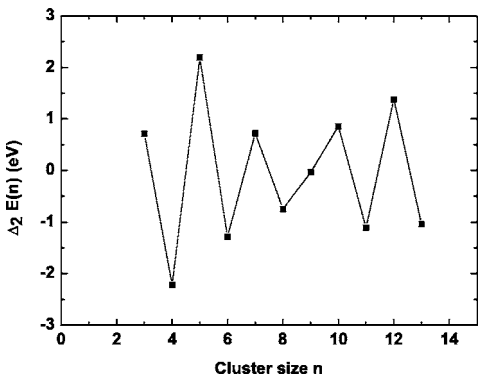

FIG. 3. The second differences of Si_nFe cluster energies for the lowest-energy structures $\Delta_2E(n)$ as a function of the cluster size n.

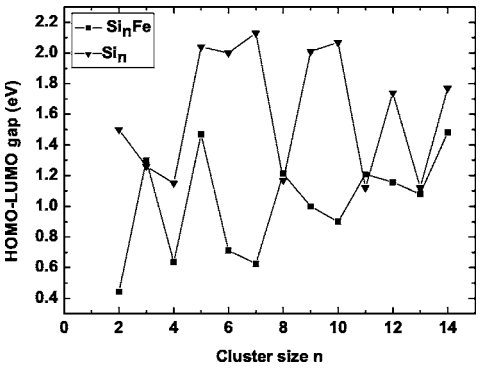

FIG. 4. Size dependence of HOMO-LUMO gaps of Si_nFe and Si_n clusters for the lowest-energy structures.

In cluster physics, the second-order difference of cluster energies, $\Delta_2E(n)=E(n+1)+E(n-1)-2E(n)$, is a sensitive quantity that reflect the relative stability of clusters.[37] Figure 3 shows the second-order difference of cluster total energies, $\Delta_2E(n)$, as a function of the cluster size. Maxima are found at $n=5,7,10,12$, indicating these clusters possess higher stability, which is consistent with the trend of binding energies shown in Fig. 2. A distinct structure for the stability of the clusters can also be observed in Fig. 3. For small clusters $(n\leqslant 8)$, odd n gives high stability while even n gives low stability. Around $n=9$, this behavior is inverted. From n $\geqslant 10$, even n gives more stable clusters than odd n. This indicates that $n=9$ should be the turning point for the stability of clusters.

As shown in Table I, Si_5Fe has the largest vertical ionization potential, corresponding to its higher stability. Khanna *et al.* found $Si_{10}Fe$ is more stable than its neighbors,[17] although their geometries are different from ours. They explained the higher stability of $Si_{10}Fe$ using the 18-electron rule. However, it should be pointed out that the 18-electron rule has its certain limitation. Sen *et al.*[24] found that filling of electron shell according to 18-electron rule is not the only factor in determining the cluster stability. The stability depends on other factors such as geometry structure, the size of metal atom, etc. For example, closed-cage configuration like the pentagonal or hexagonal prism of Si_{10} and Si_{12} might contribute the higher stability of the Fe-doped clusters.

As shown in Fig. 4, the HOMO-LUMO gaps of Si_nFe clusters are usually smaller than those of Si_n clusters except that the gaps are close to each other at $n=3,8,11,13$, (Fig. 4).[26,27] To further understand this effect, we have performed detailed analysis of the molecular orbitals by examining the partial density of states from the contribution of different orbital components (s,p,d) and the electron density of the HOMO and LUMO states. Figure 5 gives the partial density of states (PDOS) of some Si_nFe clusters (Si_3Fe, Si_4Fe, $Si_{12}Fe$, $Si_{14}Fe$) as representative. It can be clearly seen that the electronic states at the vicinity of Fermi level are mainly come from p and d states and the contribution from s state is very little. Similar behavior was observed for all the other sized clusters. The distribution of electron density of HOMO

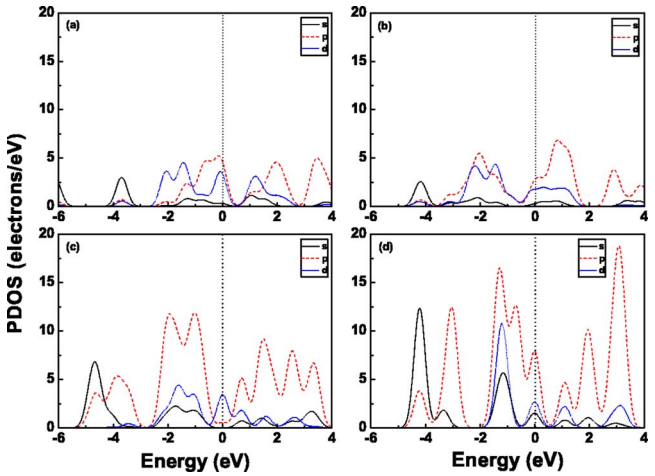

FIG. 5. (Color online) The partial density of states (PDOS) of *s*, *p*, and *d* orbitals for (a) Si_3Fe, (b) Si_4Fe, (c) $Si_{12}Fe$, and (d) $Si_{14}Fe$. The vertical line indicates the Fermi level.

and LUMO states of these representative clusters (Si_3Fe, Si_4Fe, $Si_{12}Fe$, $Si_{14}Fe$) are plotted in Fig. 6. One can see that both the HOMO and LUMO states are mainly localized around Fe atom, while there is also some distribution around Si atoms. The Figs. 5 and 6 together, indicate that the

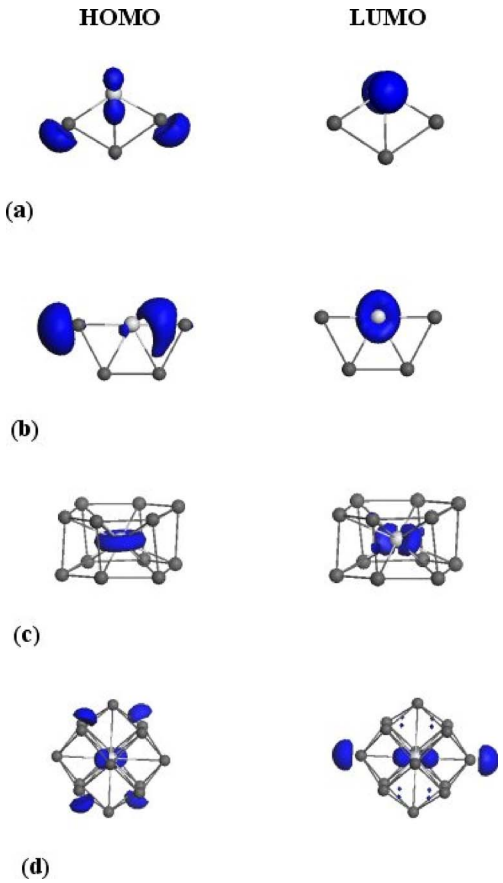

FIG. 6. (Color online) The HOMO and LUMO orbitals of (a) Si_3Fe, (b) Si_4Fe, (c) $Si_{12}Fe$, and (d) $Si_{14}Fe$. The iso-value=0.05. In (b), the HOMO does not reflect the symmetry of the cluster. This may indicate that the HOMO is actually degenerate.

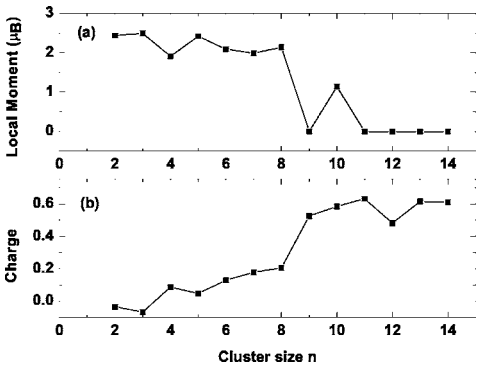

FIG. 7. Size dependence of (a) magnetic moment and (b) atomic charges of Fe atom of Si_nFe clusters for the lowest-energy structures.

HOMO and LUMO are composed of Fe *d*-states mixed with Si *p*-states. Thus, *pd*-hybridization should be responsible for the reduction of HOMO-LUMO gap with addition of Fe. This effect may provide a valuable pathway of controlling the HOMO-LUMO gap by appropriately choosing a transition metal atom and doping it inside the silicon clusters.[17]

We performed Mulliken population analysis for the lowest-energy structures and the atomic charges of Fe atom of the clusters $FeSi_n$ are listed in Table I and plotted in Fig. 7. For the smallest clusters with $n=2$ and 3, there is weak charge transfer from Fe atom to Si atoms. Starting from $n=4$, the direction of charge transfer reverses and the amount of charges transfer from Si atoms to Fe atoms increase with increasing cluster size. There is an abrupt increase of charge transfer from $FeSi_8$ to $FeSi_9$, and the size-dependence of charge transfer exhibits two-steps behavior at $FeSi_4$ to $FeSi_8$ and $FeSi_9$ to $FeSi_{14}$.

Based on the optimized geometries, the magnetic properties of $FeSi_n$ clusters were computed and the results are presented in Table I and Fig. 7. For smaller $FeSi_n$ clusters with $n=2-8$, the total magnetic moment of cluster is about 2.0 to 2.5 μ_B and is mainly located on the Fe site. Small amount of spin (about 0.02–0.2 μ_B) was found on the Si sites, while most of the local moments on Si atoms were found to align antiferromagnetically with respect to that on Fe atom. However, the magnetic moment of Fe atom in Si_nFe clusters is quenched around $n=9$ to 10. Larger Si_nFe clusters with $n=9$, 11–14 are completely nonmagnetic, whereas $Si_{10}Fe$ has a magnetic moment of 1.140 μ_B. Sen *et al.*[24] studied the TM atom encapsulated in a Si_{12} hexagonal prism cage and found that $Si_{10}Fe$ and $Si_{12}Fe$ adopt singlet as ground states. Lu *et al.*[18] also found that $Si_{10}Fe$ is magnetic while their computed moment is 2 μ_B for $FeSi_{10}$.

In our study, detailed analysis of the on-site atomic charges and local magnetic moment was performed. The charge and spin of 3*d* and 4*s* states for Fe atom in Si_nFe clusters are summarized in Table II. It clearly shows that the magnetic moment of the Fe atom is mainly due to 3*d* state of Fe. For free Fe atom, the configuration of valence electrons is $3d^64s^2$. In the cases of Si_nFe clusters, the 3*d* state gain extra electrons, meanwhile the 4*s* state loses some amount of electrons (Table II). Namely, there is internal electron transfer from 4*s* state to 3*d* state in Fe atom. On the whole, the 3*d*

TABLE II. The charge and magnetic moment of $3d$ and $4s$ states for Fe atom in Si_nFe clusters.

	$3d$		$4s$	
n	Charge	Magnetic moment	Charge	Magnetic moment
2	6.928	2.231	0.808	0.174
3	6.923	2.355	0.667	0.118
4	6.988	1.717	0.625	0.098
5	6.906	2.278	0.736	0.111
6	6.975	1.927	0.713	0.157
7	7.006	1.799	0.672	0.148
8	6.974	2.007	0.660	0.095
9	7.129	0.000	0.681	0.000
10	7.097	1.101	0.685	0.004
11	7.213	0.000	0.682	0.000
12	7.121	0.000	0.681	0.000
13	7.197	0.000	0.710	0.000
14	7.156	0.000	0.749	0.000

state gains more electrons for the spin-quenched sizes than the size with unquenched spin. As mentioned above (Table I and Fig. 7), for the smallest clusters with $n=2$ and 3, there is weak charge transfer from Fe atom to Si atoms. Starting from $n=4$, the direction of charge transfer reverses and the amount of charges transfer from Si atoms to Fe atoms increase with increasing cluster size. This indicates that besides the internal electron transfer in Fe atom, there is also the charge transfer between Fe and Si atoms. For the Si_nFe clusters, the charge transfer mainly happens between Fe $4s$, $3d$ and Si $3s$, $3p$ states. Figure 7 plotted the magnetic moment of Fe atom, along with the on-site charge on Fe atom. It can be clearly seen that there is a correspondence between the abrupt increase of charge transfer and the quenching of magnetic moment at $n=9$. This result implies that the charge transfer and the strong hybridization between Fe $4s$, $3d$ and Si $3s$, $3p$ states might be one major reason for quenching the magnetic moment of Fe atom. Similar phenomenon was observed in Cr atom encapsulated in Si cages.[16] On the other hand, the transition size for the formation of Si cage is around $n=9$ to 10. Thus, there might be some correlation between the geometry structure of Si framework and the magnetic moment of the encapsulated Fe atom.

V. CONCLUSION

A systematic theoretical study on the growth behavior and magnetic properties of Si_nFe ($n=2-14$) clusters has been performed using DFT-GGA calculations. For each cluster size, an extensive search of the lowest-energy structures has been conducted by considering a number of structural isomers. In the ground-state structures of Si_nFe clusters, the equilibrium site of Fe atom gradually moves from convex, surface, to interior sites as the number of Si atom varying from 2 to 14. Starting from $n=10$, Fe atom completely falls into the center of the Si outer frame, forming metal-encapsulated Si cages. From the analysis of second-order energy difference, Si_nFe clusters at $n=5,7,10,12$, possess relatively higher stability. The electronic structures and magnetic properties of these Si_nFe clusters in their ground-state structures were discussed. We find that the magnetic moment of Fe atom in Si_nFe clusters is quenched around $n=9$ to 10, due to the charge transfer and strong hybridization between $4s$ and $3d$ states of Fe and $3s$ and $3p$ states of Si.

ACKNOWLEDGMENTS

This work was financially supported by the National Natural Science Foundation of China (Grants Nos. 90206033, 10274031, 60478012, 10474030, 90406024), the Foundation for the Author of National Excellent Doctoral Dissertation of PR China (Grant No. 200421), the Office of Naval Research (US) under Grant No. N00014-01-1-0802, and the Department of Energy (US) under Grant No. DEFG0397SF21388.

*Corresponding author. Email address: zhojj@dlut.edu.cn

[1] M. F. Jarrold, Science **252**, 1085 (1991); M. F. Jarrold and J. E. Bower, J. Chem. Phys. **96**, 9180 (1992).

[2] M. F. Jarrold and V. A. Constant, Phys. Rev. Lett. **67**, 2994 (1991); R. R. Hudgins, M. Imai, M. F. Jarrold, and P. Dogourd, J. Chem. Phys. **111**, 7865 (1999).

[3] K. Raghavachari and C. M. Rohlfing, J. Chem. Phys. **89**, 2219 (1988); K. M. Ho, A. A. Shvartsburg, B. Pan, Z. Y. Lu, C. Z.

Wang, J. G. Wacker, J. L. Fye, and M. E. Jarrold, Nature (London) **392**, 582 (1998); K. A. Jackson, M. Horoi, I. Chaudhuri, T. Frauenheim, and A. A. Shvartsburg, Phys. Rev. Lett. **93**, 013401 (2004).

[4] S. Yoo, J. J. Zhao, J. L. Wang, and X. C. Zeng, J. Am. Chem. Soc. **126**, 13845 (2004); J. L. Wang, X. L. Zhou, G. H. Wang, and J. J. Zhao, Phys. Rev. B **71**, 113412 (2005); J. Zhao, J. Wang, J. Jellinek, S. Yoo, and X. C. Zeng, Eur. Phys. J. D **34**, 35 (2005).

[5] S. M. Beck, J. Chem. Phys. **90**, 6306 (1989).

[6] H. Hiura, T. Miyazaki, and T. Kanayama, Phys. Rev. Lett. **86**, 1733 (2001).

[7] M. Ohara, K. Koyasu, A. Nakajima, and K. Kaya, Chem. Phys. Lett. **371**, 490 (2003).

[8] K. Koyasu, M. Akutsu, M. Mitsui, and A. Nakajima, J. Am. Chem. Soc. **127**, 4998 (2005).

[9] V. Kumar and Y. Kawazoe, Phys. Rev. Lett. **87**, 045503 (2001).

[10] V. Kumar and Y. Kawazoe, Phys. Rev. B **65**, 073404 (2002).

[11] V. Kumar and Y. Kawazoe, Appl. Phys. Lett. **83**, 155412 (2003).

[12] H. J. W. Zandvliet, R. Van Moere, and B. Poelsema, Phys. Rev. B **68**, 073404 (2003).

[13] H. Kawamura, V. Kumar, and Y. Kawazoe, Phys. Rev. B **70**, 245433 (2004).

[14] H. Kawamura, V. Kumar, and Y. Kawazoe, Phys. Rev. B **71**, 075423 (2005).

[15] A. K. Singh, V. Kumar, and Y. Kawazoe, Phys. Rev. B **71**, 115429 (2005).

[16] S. N. Khanna, B. K. Rao, and P. Jena, Phys. Rev. Lett. **89**, 016803 (2002).

[17] S. N. Khanna, B. K. Rao, P. Jena, and S. K. Nayak, Chem. Phys. Lett. **373**, 433 (2003).

[18] J. Lu and S. Nagase, Phys. Rev. Lett. **90**, 115506 (2003).

[19] M. Menon, A. N. Andriotis, and G. E. Froudakis, Nano Lett. **2**, 301 (2002).

[20] A. N. Andriotis, G. Mpourmpakis, G. E. Froudakis, and M. Menon, New J. Phys. **4**, 78 (2002).

[21] G. Mpourmpakis, G. E. Froudakis, A. N. Andriotis, and M. Menon, J. Chem. Phys. **119**, 7498 (2003).

[22] G. Mpourmpakis, G. E. Froudakis, A. N. Andriotis, and M. Menon, Phys. Rev. B **68**, 125407 (2003).

[23] T. Miyazaki, H. Hiura, and T. Kanayama, Phys. Rev. B **66**, 121403(R) (2002).

[24] P. Sen and L. Mitas, Phys. Rev. B **68**, 155404 (2003).

[25] P. Guo, Z. Ren, F. Wang, J. Bian, J. Han, and G. H. Wang, J. Chem. Phys. **121**, 12265 (2004).

[26] F. Hagelberg, J. Leszczynski, and V. Murashov, J. Mol. Struct.: THEOCHEM **454**, 209 (1998).

[27] L. Ma, J. J. Zhao, J. G. Wang, Q. L. Lu, L. Z. Zhu, and G. H. Wang, Chem. Phys. Lett. **411**, 279 (2005).

[28] G. Mpourmpakis, G. E. Froudakis, A. N. Andriotis, and M. Menon, Phys. Rev. B **68**, 125407 (2003).

[29] S. A. Wolf, D. D. Awschalom, R. A. Buhrman, J. M. Daughton, S. von Molnár, M. L. Roukes, A. Y. Chtchelkanova, and D. M. Treger, Science **294**, 1488 (2001).

[30] B. Delley, J. Chem. Phys. **92**, 508 (1990).

[31] J. P. Perdew and Y. Wang, Phys. Rev. B **45**, 13244 (1992).

[32] R. S. Mulliken, J. Chem. Phys. **23**, 1841 (1955).

[33] J. L. Wang, G. H. Wang, F. Ding, H. Lee, W. F. Shen, and J. J. Zhao, Chem. Phys. Lett. **341**, 529 (2001).

[34] K. Jackson, M. R. Pederson, D. Porezag, Z. Hajnal, and T. Frauenheim, Phys. Rev. B **55**, 2549 (1997).

[35] B. X. Li, M. Qiu, and P. L. Cao, Phys. Lett. A **256**, 386 (1999).

[36] Z. Y. Lu, C. Z. Wang, and K. M. Ho, Phys. Rev. B **61**, 2329 (2000).

[37] J. L. Wang, G. H. Wang, and J. J. Zhao, Phys. Rev. B **64**, 205411 (2001).